Surface modification and deuterium retention in reduced-activation steels under low-energy deuterium plasma exposure

Part I: undamaged steels

O. V. Ogorodnikova[1], Z. Zhou[2], K. Sugiyama[3], M. Balden[3], Yu. Gasparyan[1], V. Efimov[1]

[1]*National Research Nuclear University 'MEPhI' (Moscow Engineering Physics Institute), Moscow, Russia*

[2]*University of Science and Technology Beijing, Beijing 100083, China*

[3]*Max-Planck Institute fuer Plasmaphysik, Garching, Germany*

Abstract

In the present work, reduced-activation ferritic/martensitic (RAFM) steels including Eurofer (9Cr) and oxide dispersion strengthening (ODS) steels by the addition of Y_2O_3 particles with different amount of Cr, namely, (9-16)Cr were exposed to low energy deuterium (D) plasma (~20-200 eV per D) up to a fluence of 2.9×10^{25} D/m^2 in the temperature range from 290 K to 700 K. The depth profile of D in steels was measured up to 8 μm depth by Nuclear Reaction Analysis (NRA) and the total retained amount of D in those materials was determined by Thermal Desorption Spectroscopy (TDS). It was found that the D retention in ODS steels is higher compared to Eurofer due to the much higher density of fine dispersoids and finer grain size. This work shows that in addition to the sintering temperature and time, the type, size, and concentration of the doping particles have an enormous effect on the increase in the D retention. The D retention in undamaged ODS steels strongly depends on the Cr content: ODS with 12Cr has a minimum and the D retention in the case of ODS with (14-16)Cr is higher compared to (9-12)Cr**.** The replacing of Ti by Al in ODS-14Cr steels reduces the D retention. The formation of nano-structure surface roughness enriched in W or Ta due to combination of preferential sputtering of light elements and radiation-induced segregation was observed at incident D ion

energy of 200 eV for both Eurofer and ODS steels. Both the surface roughness and the eroded layer enhance with increasing the temperature. The surface modifications result in a reduction of the D retention near the surface due to both sputtering of trapped D on the surface of a steel by incident D ions and increasing the desorption flux. Such surface modifications lead to a reduction in the overall D retention.

* Corresponding author: Olga V. Ogorodnikova, igra32@rambler.ru, National Research Nuclear University 'MEPHI', Kashirskoe shosse 31, 115409 Moscow, Russia

1. Introduction

Ferritic/martensitic steels are one of the candidate materials for the vessel of the spallation target [1], and reduced-activation ferritic/martensitic (RAFM) steels, such as Eurofer, are first priority materials of structure for fusion nuclear reactors [2,3]. These systems are desired to operate at relatively high temperatures up to 650 C. RAFM steels possess exceptional thermal conductivity and low thermal expansion among other steels while being strongly resistant to void swelling. The RAFM steels such as Eurofer97, F82H and Rusfer were developed in Europe [4,5], Japan [6], and Russia [7], respectively. Their composition lies in the following range: Fe-(7.5–12)Cr-(1.1–2)W-(0.15–0.25)V, in weight percent. The F82H, a nominally Fe–8Cr–2W–0.14V–0.04Ta–0.1C (without N), was originally developed by the Japan Atomic Energy Research Institute and JFE. Eurofer97, a 9Cr RAFM alloy (Fe–9Cr–1W-0.2V–0.07Ta–0.03N–0.1C), was produced by the European Union. This steel contains lower W and higher Ta concentration compared to F82H [8]. Reduction of tungsten is expected to result in a higher tritium breeding ratio and a reduction of Laves phase formation which can embrittle the steel [9,10]. Oxide dispersion strengthening (ODS) by the addition of Y_2O_3 particles has been successfully applied to improve high-temperature strength of RAFM's steels [11,12]. Dispersion of a high number density of nano-size yttria particles is also effective to reduce radiation-induced microstructural change because of the effective sink of interface between oxide particles and matrix for irradiation-induced point defects [**11-14**].

In fusion or fast breeder reactors, particles with high energy irradiate the vessels or structures, and helium and hydrogen atoms are generated in materials. The prediction of fuel retention in plasma exposed materials depends on the understanding of the fundamental retention mechanisms in these materials. In the frame of ITER project, efforts were made to introduce new data with emphasis on fuel retention in tungsten (W) with respect to a reduction of uncertainties, importance of the ion flux effect and the influence of neutron-induced damage [15-18]. These investigations confirmed that the retention in W should be small compared to

that expected for C and Be and is consequently not considered to be a major concern for ITER operation. Although a lot of literature exist about hydrogen embrittlement in stainless steel, not much efforts have been done to investigated the deuterium (D) retention in ODS steels facing the plasma.

In the present work, the accumulation of D in RAFM's steels with different chemical compositions and structure is investigated under well-defined laboratory conditions. Eurofer (~9Cr) and ODS steels with different amount of Cr, namely, from 9Cr to 16Cr, were exposed to low energy (~20-200 eV per D) deuterium plasma up to a fluence of ~2.9×10^{25} D/m^2 at different sample temperatures. After the plasma exposure, the post-mortem analysis was carried out including a) Scanning Electron Microscopy (SEM) equipped with Energy-Dispersive X-Ray Spectroscopy (EDX) to see surface modification and surface composition, b) Rutherford backscattering spectroscopy (RBS) for the analysis of surface elemental composition, c) the depth profile of D in steels up to 8 μm in depth by Nuclear Reaction Analysis (NRA) and d) the total retained amount of D in those materials was determined by Thermal Desorption Spectroscopy (TDS).

2. Experimental

2.1. Material and Samples

Ferritic/martensitic steels with low-activation and high resistance to void swelling, such as Eurofer and ODS steels, are the most promising candidate materials for structural components for fusion and advanced fission power generation reactors. In the past, bare MANET and Eurofer steels were considered to be a first wall for a DEMO reactor [19].

The mechanical and physical properties, the effect of alloying and the effect of heat treatments on Eurofer variants have been widely studied [4, 20–23]. The heat treatment during manufacturing was the following. First, 980°C for 30 minutes that results in a formation of typically 10 μm large austenite grains. Then cooling with a rate faster than 5K/min down to end

of martensite formation, i.e. 215°C leads to a formation of martensite from undercooled austenite (high cooling rate required for suppression of carbon diffusion). Finally, annealing to 750°C for 2h results in a slight reduction of hardness and brittleness by controlled carbon diffusion and formation of metal carbides. The main important compositions are ~9Cr, 1W, 0.14Ta, 0.2V and 0.12C [4,22] (**Table 1)**.

Fe–(9–16)Cr–2W-0.15Si-0.5Ti–0.35Y_2O_3 alloys (in weight percent) have been manufactured in China by mechanical alloying followed by HIPping (100 MPa, 1150 °C, 3h) and forging (initial temperature 1150-1170 °C, final temperature 970 °C, forging ratio 3:1) [**24]**. The chemical compositions are presented in **Table 1**. Fe-(9-12)Cr has ferritic/martensitic structure and Fe-(14-16)Cr has ferritic structure. In some set of ODS-14Cr steels, Ti was replaced by Al. According to [**12**], an increase of Cr and an addition of Al at the same time resulted in suppression of corrosion. However, too high Cr content will cause the precipitation of Cr-enriched segregation phase, which is detrimental to the ductility of ODS ferritic steels [**24,25**].

All samples were cut from larger blocks after the respective heat treatment. Thereafter they were gridded and polished to mirror finish. The size of samples after polishing was 10x10x(0.5-1) mm^3 in the case of ODS and 12x15x(0.5-1) mm^3 in the case of Eurofer.

The surface morphology of those steels was examined by SEM equipped with EDX for chemical surface analysis. SEM images of Eurofer 'as received' and annealed in a vacuum up to 1000 K are shown in **Fig. 1**.

The general microstructure of Eurofer consists of equiaxed and elongated grains. The mean grain size obtained by SEM is typically from one to ten μm and does not noticeably change with heat treatment up to 1000 K. The microstructure of Eurofer steel is ferritic/martensitic with precipitates both at grain boundaries and to a lesser extent within the grains. The elemental analysis suggests that the precipitates are $M_{23}C_6$ [**20,23**] which can contain tantalum, tungsten, chromium, vanadium, etc. The density of precipitates on the grain

boundaries increases after annealing up to 1000 K. We found some Ta-rich carbides, W-rich carbides and few V-rich carbides after annealing of Eurofer at 1000 K. This is in agreement with [**20]**. Randomly distributed regions of large ferritic grains retained after the heat treatments as it was also mentioned in [**20]**. Transmission electron microscopy (TEM) analysis confirms the microstructural analysis suggested by SEM, showing ferritic matrix with carbides precipitated at grain boundaries (GBs) and within the grains in all the heat-treated samples [**23**].

The microstructure of ODS steel produced in China [**24**] is rather complicated and considerably differs from Eurofer samples. The structure is very inhomogeneous with Ti –Cr precipitates, probably, in the form of oxides, some of them contain Y (small ones), some W (big ones) and there are also SiO_2 dispersoids (biggest ones). ODS steels contained precipitates of mean size of about 200 nm, 20–30 nm and 3-5 nm. For all the specimens, a large amount of homogeneously distributed ultrafine oxide particles in the form of Y–Ti–O were observed in [**24]**, with a size ranging from several nm up to ~50 nm. The mean grain size obtained by SEM and TEM [**24]** for ODS steels is from less than one up to several μm that is smaller or comparable with mean grain size of Eurofer.

2.2. Plasma exposure

Samples were exposed to the D plasma generated by an electron-cyclotron resonance (ECR) plasma source in the experiment PLAQ which delivers mostly D_3^+ (97%) ions [**26**]. Up to six samples were exposed simultaneously to deuterium plasmas in order to have identical experimental conditions. A d.c. bias of - 60 V and -600 V were applied to the substrate holder to accelerate the ions in the sheath leading to an energy of about 60 eV per ion and 600 eV per ion, respectively. In general, there is a plasma potential of several volts but we do not take it into account because its insignificant contribution. Because the main component of the flux is D_3^+, the sample bias of -60 eV produces ions with a mean energy of 20 eV per deuteron and the sample

bias of -600 V produces ions with a mean energy of 200 eV per deuteron. The deuteron flux was about 10^{20} D m^{-2} s^{-1}.

2.3. Post-mortem analysis

The post-mortem analysis was performed using a) SEM equipped with EDX to see surface modification, b) RBS for the analysis of surface elemental composition, c) NRA using ^{3}He as analysing ion beam to measure the depth profile of D in steels up to 8 μm in depth and d) TDS to define the total retained amount of D in those materials. The samples were stored in vacuum between the measurements.

The D concentration within the near-surface layer (at depths of up to ~0.6 μm) was measured by means of the D(^{3}He,α)H reaction at a ^{3}He energy of 0.69 MeV, and the α particles were energy-analyzed with a small-angle detector at a laboratory scattering angle of 102°. The α spectrum was transformed into a D depth profile using the code SIMNRA [27]. The D concentration at larger depths was evaluated by means of the D(^{3}He,p)^{4}He reaction with an analyzing beam of ^{3}He ions with energies varied from 0.69 to 4 MeV. The D(^{3}He,p)^{4}He nuclear reaction has a resonant-like cross-section with a broad maximum at around 0.63 MeV. Several different ^{3}He incident energies were chosen for the measurement, taking the depth resolution for D in steel into account. The energy spectra of emitted protons produced by the D(^{3}He,p)^{4}He nuclear reaction for all different ^{3}He energy were measured using a surface barrier proton detector placed at an angle of 135°. The D concentration profile was then determined by using SIMNRA to fit its calculated proton spectra to experimental ones. Details of this procedure can be found elsewhere, see, for example [**18**]. Usually, NRA was performed from several days to several months after the plasma exposure.

Total D retention in samples was analyzed by means of TDS in ultra-high vacuum chamber with the base pressure of less than 2×10^{-7} Pa [**28]**. The samples were heated resistively

up to 1400 K with a linear ramp of 2 K/s. The temperature was measured by the thermocouple directly welded to the sample. Release of deuterium was controlled by quadrupole mass-spectrometer PFEIFFER Prisma QME 200. Twenty different masses including important masses of H_2, HD, D_2, HDO, D_2O, were monitored during the whole experiment. A quadrupole mass spectrometer (QMS) was used to monitor the desorbed hydrogen molecules: mass 2(H_2), mass 3 (HD) and mass 4 (D_2), and D-related water: mass 19 (HDO) and mass 20 (D_2O). The absolute sensitivity of QMS to D_2 was routinely measured after every experiment using a system including two leak valves and baratron (see details in [**28**]). The relative sensitivity to H_2 was determined once in a separate experiment with the same procedure. The relative sensitivity for HD was taken as an average between H_2 and D_2 values. For most of the experiments mass 4 (D_2) was dominating the release spectra and absolute calibration was straightforward with an experimentally determined calibration factor for D_2. For low fluences, significant intensities on the other mass channels were also observed. Reasonable sensitivities were assumed to quantify the D release in these cases [**28**]. TDS was performed from several months up to a year after the D plasma exposure.

3. Results and discussion

3.1. Surface modification

Nano-roughness surface modification (‘grass’-like) of RAFM’s steels was observed by SEM after the D plasma exposure with 200 eV at room temperature as shown in **Fig. 2**. Because the light elements have higher sputtering yields compared to heavy elements, the heavy elements will accumulate on the surface leading to a formation of a W-rich and Ta-rich layer on the steel surface.

The cones with uneven surface in **Fig. 2** were found to be enriched in W due to preferential sputtering (PS) of light elements as it was measured with EDX and RBS. In general,

the factors causing the preferential sputtering are differences in both masses and binding energies of surface elements as well as radiation-induced surface segregation (RIS). Although ODS steels have higher concentration of W (2% by weight) compared to Eurofer (1% by weight), no visible variations in the surface roughness in different RAFM's steels was observed after irradiation with 200 eV D ions.

With increasing the sample temperature, the formation of surface roughness is enhanced and the lateral length scale is increased too, as shown in **Fig. 3**. **Fig. 3** shows SEM images of Eurofer and ODS-12Cr after exposure to the D plasma with an incident ion energy of 200 eV per D at 600 K. The same change of the surface modification with increasing the temperature was found on the different RAFM's steels, regardless of the presence of nanoparticles and Cr content. It seems that nano-scaled ODS particles do not play a role of centres for trapping of point defects and diffusing alloy elements and cannot prevent the enhanced sputtering of a steel as well as RIS and radiation-enhanced diffusion (RED) at elevated temperatures.

Fig. 4 shows an example of an increase of surface roughness of Eurofer after exposure to the D plasma with incident ion energy of 200 eV per D at 700 K compared to 290 K. It appears that the cones are coarser at 700 K (Fig. 4b) than at 290 K (Fig. 4a). This is an indication that the W is segregating in larger clusters at elevated temperatures. Since sputtering yields of metals are insensitive to temperature up to near the melting point, the temperature dependence observed is an indication of the importance of thermally-activated processes in alloy sputtering. Near room temperature, PS and Gibbsian segregation (GS) are the main processes which govern the development of the surface modifications and the alloy composition in the layer altered by ion implantation. The altered layer extends to a depth deeper than the mean projected ion range, which is R_p=4.43 nm for an incident deuterium energy of 200 eV in Fe according to TRIM calculations. The implantation ion range is only marginally changed for steel compared to pure iron, for example, R_p=4.40 nm for 200 eV of D in Fe-9Cr according to TRIM calculations. At high temperatures, the surface modification has length much larger than the projected range of

200 eV of D ions in Fe. The increase of the thickness of the surface layer altered by ion implantation can be attributed to synergetic effect of PS and radiation-induced surface segregation (RIS) together with radiation-enhanced diffusion (RED). According to [**29**], point defects can escape the implantation zone because the significant vacancy mobility at elevated temperatures. Surface stresses due to formation of large defect concentrations may be responsible for the enhanced surface diffusion at elevated temperatures and the radiation-induced diffusion can exacerbate the surface modification. In this case, RED and RIS result in large altered layer at elevated temperatures that extends far into the bulk of the sample. Considerably larger altered layers were found for ion bombardment at elevated temperatures in [**30,31**] because pronounced solute migration and segregation take place over large distances that is in agreement with our results. Our results suggest that RIS can contribute in the sputtering process even at 290 K because the thickness of the altered layer (defined by the dimension of the surface nano-roughness) is much larger than the mean projected ion range. Pronounced changes of the alloy composition in the near-surface region can affect the alloy sputtering.

The surface enrichment in W measured by EDX and RBS are shown in **Fig. 5** and **Fig. 6,** respectively. The W concentration on the surface increases with increasing the temperature. It seems that W particles play a role of nucleation sites or 'seeds' for further segregation of W in larger clusters at elevated temperatures due to radiation-induced diffusion of the surface atoms to the nucleation centers (RIS) that leads to a formation of 'fiber-like' surface modification. However, the surface enrichment of W cannot significantly protect the surface layer from further sputtering at elevated temperatures compared to the room temperature because Fe, Cr and other light elements can diffuse through the porous layer of W enrichment towards the surface and be sputtered or may segregate on the W-rich cones, thus, increasing the sputtering yield and surface roughness, respectively. Moreover, Si was detected on Eurofer surface after the plasma exposure. Si can be introduced on a sample surface by polishing prior exposure or can be sputtered from the nearest ODS steel specimens exposed simultaneously and re-deposited

on the Eurofer sample. The Si shows enrichment at the irradiated surface and Si-rich places can be the segregation centers for precipitation of diffusive solutes.

The surface roughness was stable by keeping for one year in vacuum at room temperature but such 'grass'-like surface modification vanishes by annealing up to 1200 K during TDS measurements (**Fig. 7**), probably, because the alloying elements diffusing to the surface during TDS restore the surface layer.

3.2. Deuterium retention

One question is: does a formation of 'nano-roughness' influence the D retention? To answer this question, samples were exposed to the D plasma with incident ion energies of 20 and 200 eV per D up to a fluence of $6x10^{24}$ D/m^2. The D retention was determined by integration of the D release over the time from TDS data. **Fig. 8** shows the D retention as a function of the sample temperature at irradiation with 20 eV D ions where the formation of nano-roughness was not observed and with 200 eV D ions where the formation of nano-roughness occurs. The D retention in steels is reduced with formation of surface roughness (or increasing of ion energy from 20 to 200 eV per D) for all investigated temperatures, namely, from 290 K to 700 K. The reduction of the D retention due to surface roughness is more pronounced at high temperatures when the growth of roughness is increased. The reduction of the D retention with the surface modifications under 200 eV D ion irradiation can be attributed to *both sputtering of trapped D from the surface of a steel by incident D ions and* an increase of the desorption flux which results in the decrease of the D concentration near the surface, thus, decreasing the diffusion flux into the bulk. The increase in the desorption flux can be due to both increased surface area and increased recombination coefficient. Indeed, the decrease of the near surface D concentration in steels irradiated with 200 eV D ions compared to 20 eV D ions was measured by NRA as shown in **Fig. 9**. **Fig. 9** shows depth profiles of D in Eurofer samples

irradiated with 20 and 200 eV per D at 290 K. The D concentration near the surface in Eurofer irradiated with 20 eV D^+ is higher compared to 200 eV D^+ due to surface modification in the case of sputtering with 200 eV D^+ (see **Figs. 2-4**).

It is important to mention that the D depth profile in steels is surprisingly inhomogeneous. The deuterium concentration in Eurofer measured up to 6 μm has four sharp maximum, at a depth of ~1, ~2.2, ~4 and ~5.5 μm (**Fig. 9**). All four peaks with only slight difference are presented in the D depth profile for all investigated steels exposed to the D plasma near the room temperature as shown in **Fig. 10.** We attribute such peaks to weakly bounded D, for example, on grain boundaries. Such weakly bounded D, most probably, is desorbed or diffuses into the bulk during the time stored the sample in vacuum after the plasma exposure. **Fig. 11** shows the D depth profiles measured in two weeks and four months after the D plasma exposure. The depth profile measured after four months is smooth without sharp maximum. Therefore, weakly bounded D was desorbed or diffused into the bulk far away from the measured depth of 6 μm to be de-trapped in more strong trapping sites with high binding energies. The D retention in RAFM steels up to 6 μm decreases by a factor of two in four months after the D plasma exposure. This means that TDS measurements after several months of time delay between the plasma exposure and start of TDS underestimates the D retention. Such change of the D depth profile was never observed in the case of W or Mo.

Fig. 12 shows a comparison of the total D retention measured by TDS in different RAFM's steels. The D retention is from two to ten times higher in ODS steels compared to Eurofer due to the high density of defects in ODS. The higher D retention in ODS steels compared to Eurofer can be connected with an increase of density of fine dispersoids and also with slight increase of the number of grain boundaries in ODS steels. The interfaces of nano-particles in ODS steels can serve as trapping sites for deuterium increasing the D retention in ODS steels. Eurofer has grain size from one to tens μm while the average grain size of ODS

steels is varied from several hundred nanometers to several μm [**24,25,32**] leading to an increase of the number of grain boundaries in ODS steels. Therefore, the decrease of the mean grain size in ODS steels compared to Eurofer should be also one from the reasons for the higher D retention in ODS steels compared to Eurofer.

We can compare the D retention in RAFM steels with that in W which is another plasma-facing material widely investigated in the laboratory conditions **[17,18,33**], used in the present tokamaks [**34,35**] and proposed to be used in ITER [**36**]. The comparison of the D retention in polycrystalline W ITER grade and ODS steels is shown in **Fig. 12**. W ITER grade is tungsten with grains elongated preferentially perpendicular in respect to the plasma-facing side. It is produced by Plansee and have a purity of 99.99 wt.% with main impurities being Mo, Fe, C and O (for details see [**18,33**]). The D retention can achieve 10^{21} D/m^2 in the case of ODS-16Cr exposed to the D plasma at room temperature that is higher than the D retention in a bulk W [**33].** In the case of ODS-16Cr, the D retention decreases up to $5x10^{19}$ D/m^2 at 700 K that is similar to the D retention in W at 700 K as reported in [**33**]. However, the TDS from ODS steels was measured many months after the D plasma exposure that can result in an underestimation of the D retention compared to *in-situ* measurements or post-mortem measurements several days after the D plasma exposure. Therefore, the D retention in ODS-(14-16)Cr steels can be even higher than the D retention in W. The D retention in Eurofer and ODS-12Cr steels is lower compared to the D retention in W at the fluence of $6x10^{24}$ D/m^2. However, due to high 'effective' diffusion of D in steels, the thickness of a sample can play a significant role for the determination of the D retention by increasing the D retention in thick sample at high fluences and moderated and elevated temperatures in contrast to the D retention in W where the 'effective' diffusion is relatively slowly and the D does not reach the downstream surface for 1 mm thick sample even at 700 K and fluence up to $6x10^{24}$ D/m^2. Using the term 'effective' diffusion, we mean the diffusion in the presence of defects [**37**] because the defects strongly delay the diffusion rate as in the case of W [**17,18**].

In contrast to the steels, the increase of the ion energy from 20 to 200 eV causes the increase in the D retention in W [**18,33**] because of different regime of the D migration and trapping in W [**18]**. In the case of W, the deuterium retention is limited by de-trapping from defects rather than to be limited by surface effects [**18,38]** while in the case of steels, the D retention is surface-limited [**18**] at least for the present experimental conditions. The effect of surface conditions on the D permeation and retention in steels in different regimes was analyzed in [**39**].

The total retention can be presented as the sum of the near surface retention (up to 3 μm) and the bulk retention

$$Ret\_total = Ret\_surf + Ret\_bulk \quad (2)$$

For the thin enough samples (0.5-1 mm), the surface retention, Ret_surf, can significantly influence the total D retention. In this case, the reduction of the D retention with a formation of surface roughness is observed as one can see in **Fig. 8**. However, the sufficient increase of the sample thickness can reduce or even eliminate the effect of the surface roughness on the D retention because in this case the bulk retention, Ret_bulk, can dominate the total D retention, especially in the case of high fluence and high sample temperature. The present sample thicknesses of 0.5-1 mm were still not too large to observe the surface effects. In the case of thick samples, Ret_bulk>> Ret_surf at high enough fluence or temperature and the surface-limited regime can be transformed in the diffusion-limited **[37,38].**

In the case of relatively high temperatures or relatively high fluences, the permeation of D through our samples with thickness of 0.5 mm occurs. The permeation was detected by NRA measurement of the D concentration on the downstream side. This means that taking thin samples, the D retention is underestimated in steels due to permeation. For this reason, the comparison of the D retention in **Fig. 12** was done for the sample thicknesses of 1 mm where no D was detected on the downstream side in the case of the D plasma exposure at 290 and 600 K. In the case of 700 K, the D concentration at downstream surface was not measured. **Fig. 13** shows an example of an increase of the D retention by a factor of about two in sample with 1

mm thickness compared to that one with 0.5 mm of thickness after exposure of samples to the D plasma with 20 eV per D at temperature of 600 K up to a fluence of $6x10^{24}$ D/m^2. In such experimental conditions, the permeation through 0.5 mm sample occurs. The permeation was also detected in other experiments described in the following paper [**40]**.

Thermal desorption spectra of deuterium from steels exposed to D plasma with 20 eV per D at room temperature up to a fluence of $2.9x10^{25}$ D/m^2 show two main desorption peaks, the peak with high amplitude at the temperature of around 560 K and the peak with low amplitude at ~790 K, and two implicit broad peaks of ~980 and ~1140 K (**Fig. 14**). All four peaks are present in TDS for both Eurofer and ODS steels indicating that the dominant trapping sites for D are similar for both kinds of steels. The increase of fine dispersoids in ODS steels enhances the density of already dominant defects from intrinsic traps in steels. While main energies of desorption are similar for all kinds of steels, the density of defects is varied depending on the steel grade. **Fig. 15** shows the dependence of the D retention on the Cr content in ODS steels. The minimum of the D retention is observed in the case of ODS-12Cr in all range of investigated temperatures.

The ODS-(14-16)Cr steels have higher D retention compared to ODS-(9-12)Cr, probably, due to a change from Ferritic/Martensitic to pure Ferritic structure. In spite that the D retention near the surface up to 6 μm can be slightly higher for ODS-12Cr compared to other ODS steels as measured by NRA in samples after exposure to the D plasma at 290 K in **Fig. 10**, the bulk D retention is lower for ODS-12Cr compared to other ODS steels. It is reasonable to suggest that there is some mechanism which reduces the diffusion of D into the bulk of ODS-12Cr or the density of defects in ODS-12Cr in the bulk is lower compared to other ODS steels.
In previous experiments described above, ODS steels with Ti dopping were used. Replacement of Ti by Al in ODS-14Cr decreases the D retention as shown in **Fig. 15**. The peak of the D release occurs at the same temperature for both ODS-14Cr-Ti and ODS-14Cr-Al steels exposed to the D plasma with 20 eV per D at 600 K as shown in **Fig. 16**. But the amount of released D is

less in the case of ODS-14Cr-Al than in the case of ODS-14Cr-Ti steel. This is because the concentration of D in the bulk of ODS-14Cr-Al is lower compared to ODS-14Cr-Ti as shown in **Fig. 17**. **Fig. 17** shows depth profiles of D in ODS steels after exposure to D plasma with ion energy of 20 eV at 600 K. An addition of Al can increase the grain size of the ODS steels as it was confirmed in [**32**]. Therefore, the number of grain boundaries reduces, thus, decreasing the D retention. One can also see in **Fig. 17** that the lowest D concentration is in ODS-12Cr-Ti at 600 K that confirms the hypothesis about a reduction of the D concentration in the bulk of the ODS-12Cr steel, resulting in the lowest total D retention in the ODS-12Cr steel. However, the reason of this reduction is unclear because no reduction of grain boundaries was observed in the case of ODS-12Cr steel compared to other ODS steels.

4. Conclusions

The surface modification of different RAFM's steels after exposure to the D plasma was investigated by SEM. The deuterium retention in different RAFM's steels was investigated by means of thermal desorption spectroscopy and nuclear reaction analysis measurements. The following observations and conclusions can be drawn.

1) The formation of similar surface roughness structure enriched in W or Ta was observed for both Eurofer and ODS steels after the exposure to the D plasma with ion energy of 200 eV. The surface roughness and sputtering yield were enhanced with increasing the temperature. The formation of surface roughness results in a decrease of the D retention near the surface due to increasing the desorption flux and can reduce the total D retention.

2) The D retention in ODS steels is higher than in Eurofer presumably due to higher density of defects in ODS steels. This work shows that the type, size, and concentration of the doping particles have an enormous effect on the D retention. The D inventory in ODS steels depends on Cr concentration: the minimum of the D retention was found in ODS-12Cr steel which was

connected, probably, with a reduction of the D diffusion into the bulk or lower density of defects in the bulk of ODS-12Cr steel compared to other ODS steels. Using Al instead of Ti in ODS-14Cr steel reduces the D retention due to a reduction of the D concentration in the bulk of the steel.

3) The addition of doping particles does not create new trapping sites for D with new binding energies but increases the density of already existing initially in RAFM steel dominant trapping sites for D.

3) The D concentration is significantly reduced in RAFM's steels after keeping the sample in vacuum for several months that results in underestimation of the retained D measured by TDS with time delay in several months after the plasma exposure.

4) The D retention can achieve 10^{21} D/m^2 in the case of ODS-16Cr exposed to the D plasma at room temperature up to a fluence of $6x10^{24}$ D/m^2 that can be higher than the D retention in a bulk polycrystalline W ITER grade exposed to the D plasma at the same conditions. In the case of ODS-16Cr, the D retention decreases up to $5x10^{19}$ D/m^2 at 700 K that is comparable to the D retention in W exposed to the D plasma in the same conditions. However, the TDS from ODS steels was measured many months after the D plasma exposure that can result in underestimation of the D retention compared to *in-situ* measurements or post-mortem measurements several days after the D plasma exposure. Moreover, the D retention in steels can be underestimated in the case of thin samples used in the present experiments due to fast D diffusion (permeation through steels was detected by NRA on the downstream side in several cases of high temperature or high fluence). Therefore, the D retention in ODS-(14-16)Cr steels can be even higher than the D retention in polycrystalline W. The D retention in Eurofer and ODS-12Cr steels was found to be lower compared to the D retention in W in the case of the plasma exposure of samples with 1 mm thickness at 20 eV $\mathbf{D}^+$ up to a fluence of $6x10^{24}$ D/m^2 in the temperature range between 290 and 700 K. It is necessary to be careful to compare the D retention in steels with the D retention in high-Z materials using the same thickness of samples.

If the D retention in W does not significantly change using either 0.5 mm or 1 mm thick samples at fluence of $6x10^{24}$ D/m^2 in the temperature range between 290 and 700 K, the D retention is lower for steel sample of 0.5 mm compared to the sample of 1 mm thick due to fast effective diffusion of D in steel that leads to permeation through steel.

5) It seems that the D retention is not a concern at least for the undamaged steels (without neutron irradiation) exposed to the D plasma at high temperatures but the D permeation through steel can be a concern **[37].**

Acknowledgement

We would like to thanks to G. Matern for the sample preparation and performing some microscopic analysis and J. Dorner and M. Fußeder for technical assistance. This work was partly supported by the Impuls- und Vernetzungsfond der Helmholtz-Gemeinschaft e.V. and partly supported by Russian Science Foundation (RSF) grant №16-12-10332. The authors also would like to express their thanks for the financial support of National Magnetic Confinement Fusion Program of China under Grant No.2015GB121006 for ODS samples preparation.

References

[1] M. Kawai, 2003 *J. Nucl. Mater*. **318** 371.

[2] A. Hishinuma, R.L. Kohyama, D.S. Klueh, W. Gelles, W. Dietz, K. Ehrlich, 1998 J. *Nucl. Mater*. **258–263** 193.

[3] L.V. Boccaccini, J.-F. Salavy, O. Bede, H. Neuberger, I. Ricapito, P. Sardain, L. Sedano, K. Splichal, 2009 *Fus. Eng. Des.* **84** 333

[4] A. Möslang, E. Diegele, M. Klimiankou, R. Lässer, R. Lindau, E. Lucon, E. Materna-Morris, C. Petersen, R. Pippan, J.W. Rensman, M. Rieth, B. van der Schaaf, H.-C. Schneider, F. Tavassoli, 2005 *Nucl. Fusion* **45** 649.

[5] C. Petersen, J. Aktaa, E. Diegele, E. Gaganidze, R. Lässer, E. Lucon, E. Materna-Morris, A. Möslang, A. Povstyanko, V. Prokhorov, J.W. Rensman, B. van der Schaaf, H.-C. Schneider, 2006, (Proc. 21st Int. Conf. Fusion Energy 2006, Chengdu, 2006) (Vienna: IAEA) CD-ROM file [IAEA, Vienna, 2007, FT/1-4Ra] and http://www-naweb.iaea.org/napc/physics/FEC/FEC2006/html/index.htm

[6] M. Tamura, H. Hayakawa, H. Tanimura, A. Hishinuma, T. Kondo, 1986 *J. Nucl. Mater*. **141** 1067.

[7] A.G. Ioltukhovskiy et al., 2005 *12th Int. Conf. on Fusion Reactor Materials (Santa Barbara)* Contribution 08-45

[8] B. van der Schaaf, D.S. Gelles, S. Jitsukawa, A. Kimura, R.L. Klueh, A. Moslang, G.R. Odette, 2000 *J. Nucl. Mater***. 283–287** 52.

[9] R.L. Klueh, D.S. Gelles, S. Jitsukawa, A. Kimura, G.R. Odette, B. van der Schaaf, M. Victoria, 2002 *J. Nucl. Mater*. **307–311** 455.

[10] S. Jitsukawa, A. Kimura, A. Kohyama, R. L. Klueh, A. A. Tavassoli, B. van der Schaaf, G. R. Odette, J. W. Rensman, M. Victoria and C. Petersen, 2004 *J. Nucl. Mater.* **329–333** 39.

[11] N. Baluc et al., 2007 *J. Nucl. Mater.* **367–370** 33

[12] A. Kimura, 2005 *Materials Transactions (Special Issue on Fusion Blanket Structural Materials R&D in Japan),* **46, No. 3** 394

[13] H. Oka, M. Watanabe, H. Kinoshita, T. Shibayama, N. Hashimoto, S. Ohnuki, et al., 2011 *J. Nucl. Mater*. **147** 279.

[14] Y. Ortega, M.A. Monge, V. de Castro, A. Munoz, T. Leguey, R. Pareja, 2009 *J. Nucl. Mater*. **386–388** 462

[15] J. Roth et al., 2009 *J. Nucl. Mater.* **390-391** 1

[16] R Neu et al., 2011 *Plasma Phys. Control. Fusion* **53** 124040

[17] O.V. Ogorodnikova, B. Tyburska, V.Kh. Alimov, K. Ertl, 2011 *J. Nucl. Mater.* **415** S661

[18] O.V. Ogorodnikova and K.Sugiyama, 2013 *J. Nucl. Mater***. 442** 518

[19] M.A. Futterer, L. Barleon, L. Giancarli, A.L. Puma, O.V. Ogorodnikova, Y. Poitevin, J.-F. Salavy, J. Szczepanski, G. Vella, 2000 *Fus. Eng. Des.* **49** 543

[20] R. Lässer, N. Baluc, J-L. Boutard, E. Diegele, S. Dudarev, M. Gasparotto, A. Möslang, R. Pippan, B. Riccardi and B. van der Schaaf, 2007 *Fus. Eng. Des.* **82** 511

[21] Z. Lu, R. G. Faulkner, N. Riddle, F. D. Martino, K. Yang, **2009** *J. Nucl.Mater.* **386–388** 445

[22] R. Lindau, A. Moeslang, M. Schirra, 2002 *Fus. Eng. Des.* **61-/62** 659

[23] S F Di Martino, R G Faulkner, N B Riddle, M A Monge and A Munoz, 2011 *Phys. Scr.* **T145** 014083

[24] Sh. Li, Zh. Zhou, J. Jang, M. Wang, H. Hu, H. Sun, L. Zou, G. Zhang, L. Zhang, 2014 *J. Nucl. Mater*. **455** 194

[25] G. Zhang, Zh. Zhou, M. Wang, Sh. Li, L. Zou, L. Zhang, 2014 *Fus. Eng. Des*. **89** 280

[26] A. Manhard, T. Schwarz-Selinger, and W. Jacob, 2011 *Plasma Sources Science and Technology* **20** 015010.

[27] M. Mayer, E. Gauthier, K. Sugiyama, U. von Toussaint, 2009 *Nucl. Instr. Meth. B* **267** 506

[28] A. Rusinov, Yu. Gasparyan, S. Perelygin, A. Pisarev, S. Stepanov, N. Trifonov, 2009 *Instruments and Experimental Techniques* **52** 871

[29] G. Was, 1990 *Progress in Surface Science* **32** 211

[30] P. Sigmund and N.Q. Lam, in: *Fundamental Processes in Sputtering*, Mat. Fys. Medd. Dan. Vid. Sdsk. (1993).

[31] L.E. Rehn, N.Q. Lam, and H. Wiedersich, 1985 *Nucl. Instrum. Methods* **B7/8** 764.

[32] M. Gong, Zh. Zhou, H. Hu, G. Zhang, Sh. Li, M. Wang, 2015 *J. Nucl. Mater.* **462** 502

[33] O. V. Ogorodnikova, K. Sugiyama, T. Schwarz-Selinger, T. Dürbeck, M. Balden, 2011 *J. Nucl. Mater.* **419** 194

[34] G.F. Matthews et al., 2009 *J. Nucl. Mater*. **390–391** 934

[35] K. Sugiyama, M. Mayer, A. Herrmann, K. Krieger, V. Rohde, M. Balden, S. Lindig, R. Neu, H.W. Müller and the ASDEX Upgrade team, 2014 *Phys. Scr.* **T149** 014043

[36] R.A. Pitts, S. Carpentier, F. Escourbiac, et al., 2013 *J. Nucl. Mater*. **438** S48

[37] O.V. Ogorodnikova, M.A. Fütterer, E. Serra, G. Benamati, J.-F. Salavy, and G. Aiello, 1999 *J. Nucl. Mater*. **273** 66

[38] O.V. Ogorodnikova, 2015 *J. Appl. Phys*, **118** 074902

[39] O.V. Ogorodnikova, 2001 *J. Nucl. Mater.* **290-293** 459

[40] O. V. Ogorodnikova, Z. Zhou, K. Sugiyama, M. Balden, G. Pintsuk, Yu. Gasparyan, V. Efimov, Part II, submitted to Nuclear Fusion

Figure captions

Fig. 1. SEM images of Eurofer: a) 'as received' and b) annealed up to 1000 K. The precipitates are $M_{23}C_6$ which can contain tantalum, tungsten, chromium, vanadium, etc. The density of precipitates on grain boundaries increases after annealing of Eurofer in a vacuum up to 1000 K.

Fig. 2. SEM images of RAFM's steels observed at 52° tilting after exposure to the D plasma with an incident ion energy of 200 eV per D at 290 K up to a fluence of $6x10^{24}$ D/m^2.

Fig. 3. SEM images of RAFM's steels observed at 52° tilting after exposure to the D plasma with incident ion energy of 200 eV per D at 600 K up to a fluence of $6x10^{24}$ D/m^2.

Fig. 4. SEM images of Eurofer observed at 52° tilting after exposure to the D plasma with incident ion energy of 200 eV per D at a) 290 K and b) 700 K up to a fluence of $6x10^{24}$ D/m^2.

Fig. 5. EDX of Eurofer after exposure to the D plasma with incident ion energy of 200 eV per D at 600 K up to a fluence of $6x10^{24}$ D/m^2 (marked as exposed) in comparison with unexposed Eurofer (marked as reference). The increase of the W with formation of nano-roughness on the surface is clearly seen.

Fig. 6. Rutherford backscattering spectra (RBS) for Eurofer samples after exposure to the D plasma with incident ion energy of 200 eV per D at sample temperatures of 290 and 700 K in comparison with unexposed Eurofer sample. The W peak indicates the surface enrichment in W.

Fig. 7. SEM images of Eurofer after exposure to the D plasma with incident ion energy of 200 eV per D at 290 K (shown in **Fig. 3a**) and then heated in a vacuum up to 1200 K with a linear ramp of 2 K/s.

Fig. 8. The D retention obtained by TDS after the D plasma exposure with incident ion energies of 20 and 200 eV per D as a function of the sample temperature under the plasma exposure in the case of a) ODS-9Cr and b) ODS-16Cr. The sample thicknesses were L=0.5 mm and fluence was $6x10^{24}$ D/m^2.

Fig. 9. Depth profiles of the D concentration in Eurofer irradiated with incident ion energies of 20 and 200 eV per D at 290 K up to a fluence of $6x10^{24}$ D/m^2.

Fig. 10. Depth profiles of the D concentration in ODS with different amount of Cr exposed to the D plasma with incident ion energy of 20 eV per D atom at 290 K up to a fluence of F=$2.9x10^{25}$ D/m^2.

Fig. 11. Depth profiles of the D concentration in ODS-9Cr steel irradiated with incident ion energy of 20 eV per D at room temperature up to a fluence of $2.9x10^{25}$ D/m^2. The measurements were performed in two weeks and four months after the D plasma exposure.

Fig. 12. A comparison of the D retention in Eurofer and ODS steels with different content of Cr with bulk polycrystalline W ITER grade [**33**] measured by TDS after the D plasma exposure with incident ion energy of 20 eV per D up to a fluence of $6x10^{24}$ D/m^2. The sample thicknesses were L=1 mm.

Fig. 13. The thermal desorption spectra of deuterium from ODS-9Cr after the D plasma exposure with incident ion energy of 20 eV per D at 600 K up to a fluence of $6x10^{24}$ D/m^2 at different sample thicknesses of 0.5 and 1 mm.

Fig. 14. Thermal desorption spectra of deuterium from steels exposed to D plasma with incident ion energy of 20 eV per D at room temperature up to a fluence of $2.9x10^{25}$ D/m^2. The TDS for Eurofer is multiplied by a factor of 10.

Fig. 15. The dependence of the D retention on the Cr content in ODS steel after exposure to the D plasma with incident ion energy of 20 eV per D at: a) 290 K, b) 600 K and c) 700 K.

Fig. 16. Thermal desorption spectra of deuterium from ODS-14Cr-Ti and ODS-14Cr-Al steels exposed to D plasma with incident ion energy of 20 eV per D at 600 K.

Fig. 17. Depth profiles of the D concentration in ODS steels after exposure to D plasma with incident ion energy of 20 eV per D at 600 K up to a fluence of F=$2.9x10^{25}$ D/m^2.

Sample	Compositions
Eurofer	Fe–9Cr–1W–0.1C-0.2V–0.14Ta–0.03N
ODS-9Cr	Fe-9Cr-1.5W-0.1C-0.15Si-0.5Ti-0.35Y_2O_3
ODS-12Cr	Fe-12Cr-2W-0.15Si-0.5Ti-0.35Y_2O_3
ODS-14Cr (Ti)	Fe-14Cr-2W-0.15Si-0.5Ti-0.35Y_2O_3
ODS-14Cr (Al)	Fe-14Cr-2W-0.15Si-**4.0Al**-0.35Y_2O_3
ODS-16Cr	Fe-16Cr-2W-0.15Si-0.5Ti-0.35Y_2O_3

Table 1. Chemical compositions of ODS versus Eurofer.

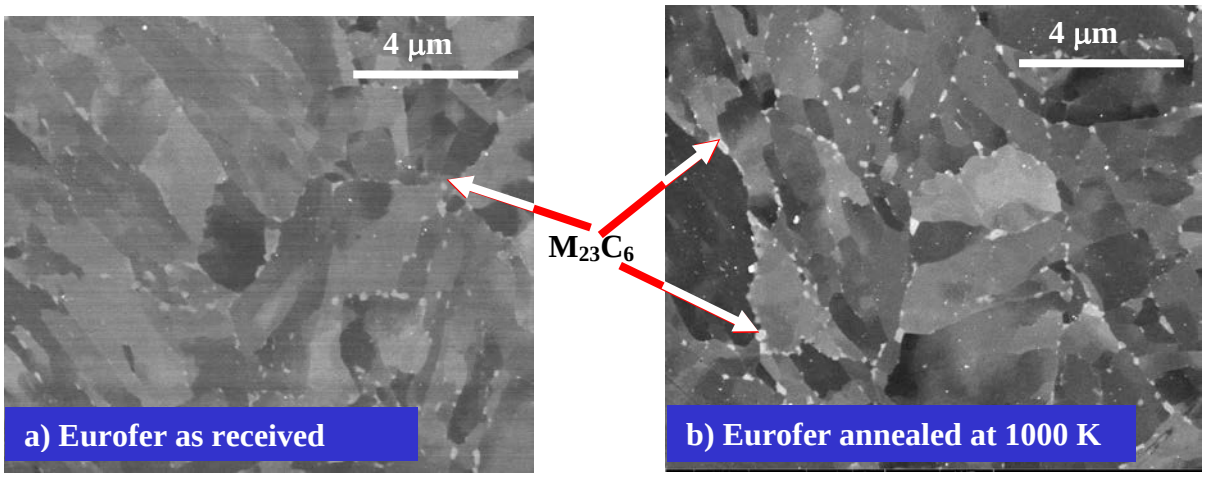

Fig. 1. SEM images of Eurofer: a) 'as received' and b) annealed up to 1000 K. The precipitates are $M_{23}C_6$ which can contain tantalum, tungsten, chromium, vanadium, etc. The density of precipitates on grain boundaries increases after annealing of Eurofer in a vacuum up to 1000 K.

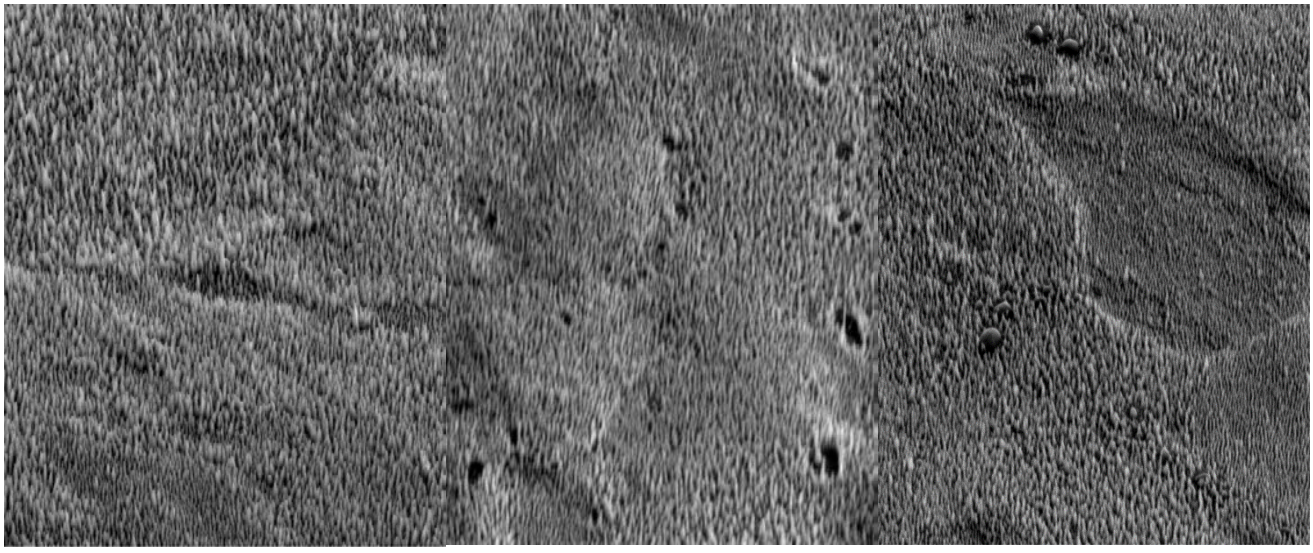

Fig. 2. SEM images of RAFM's steels observed at 52° tilting after exposure to the D plasma with an incident ion energy of 200 eV per D at 290 K up to a fluence of $6x10^{24}$ D/m^2.

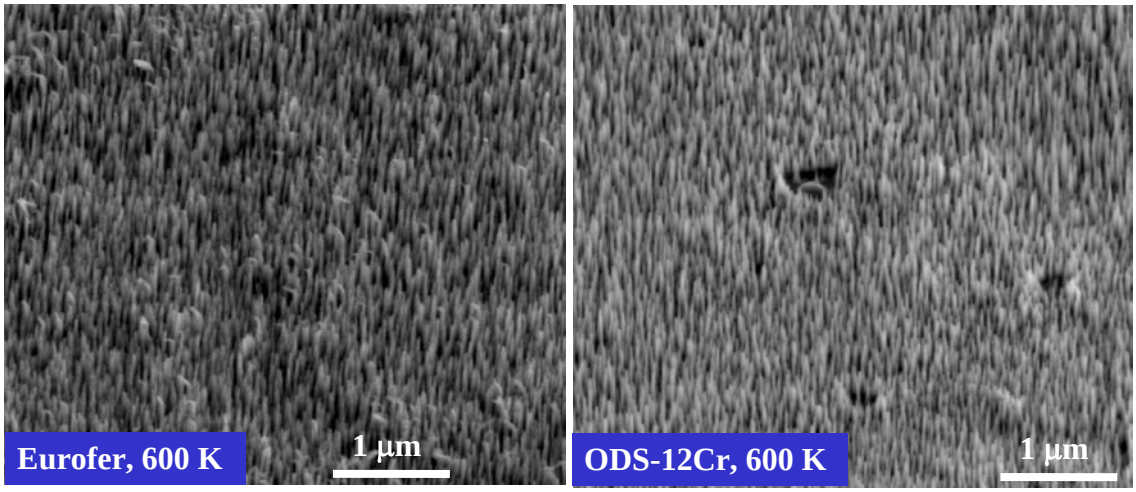

Fig. 3. SEM images of RAFM's steels observed at 52° tilting after exposure to the D plasma with incident ion energy of 200 eV per D at 600 K up to a fluence of $6x10^{24}$ D/m^2.

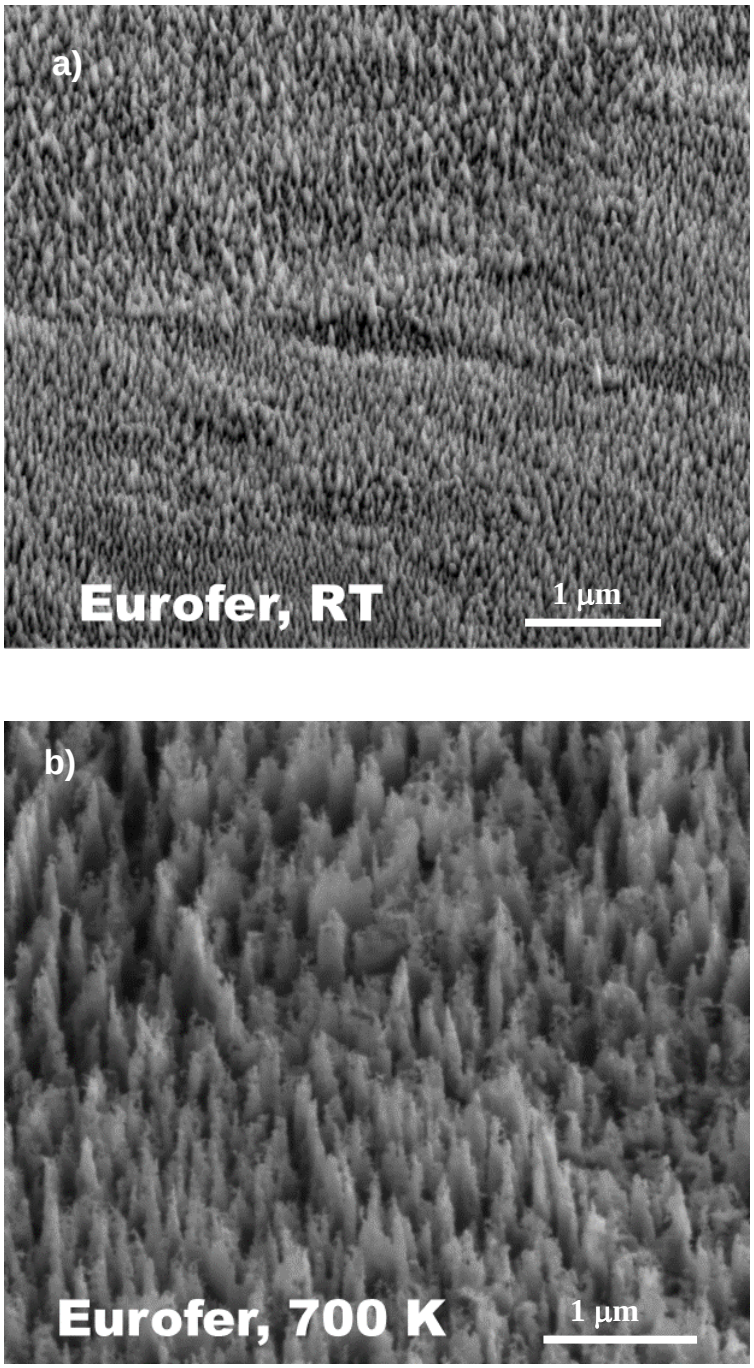

Fig. 4. SEM images of Eurofer observed at 52° tilting after exposure to the D plasma with incident ion energy of 200 eV per D at a) 290 K and b) 700 K up to a fluence of $6x10^{24}$ D/m^2.

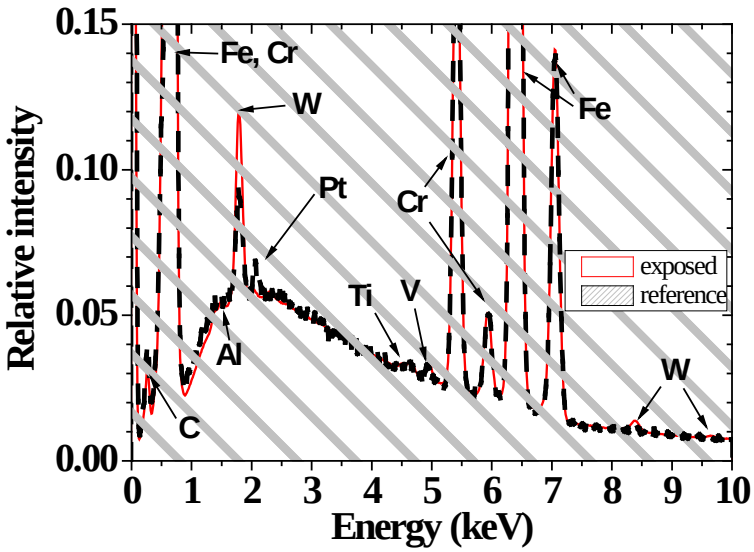

Fig. 5. EDX of Eurofer after exposure to the D plasma with incident ion energy of 200 eV per D at 600 K up to a fluence of $6x10^{24}$ D/m^2 (marked as exposed) in comparison with unexposed Eurofer (marked as reference). The increase of the W with formation of nano-roughness on the surface is clearly seen.

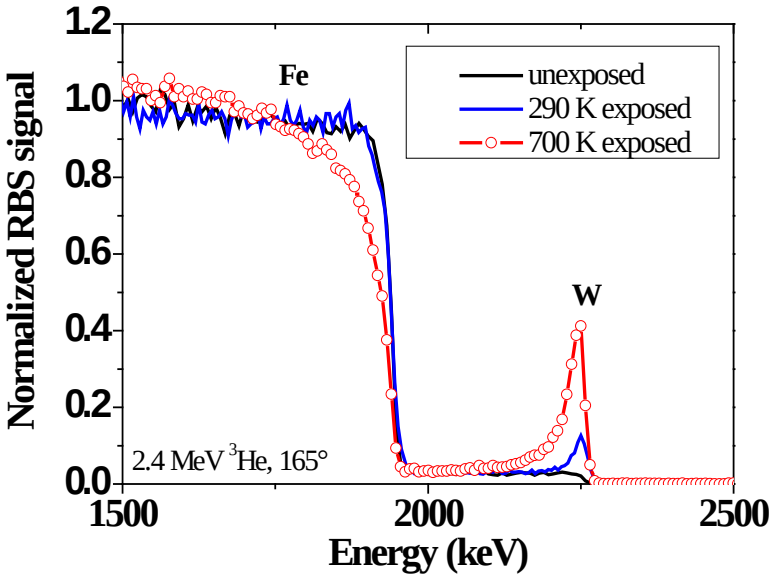

Fig. 6. Rutherford backscattering spectra (RBS) for Eurofer samples after exposure to the D plasma with incident ion energy of 200 eV per D at sample temperatures of 290 and 700 K in comparison with unexposed Eurofer sample. The W peak indicates the surface enrichment in W.

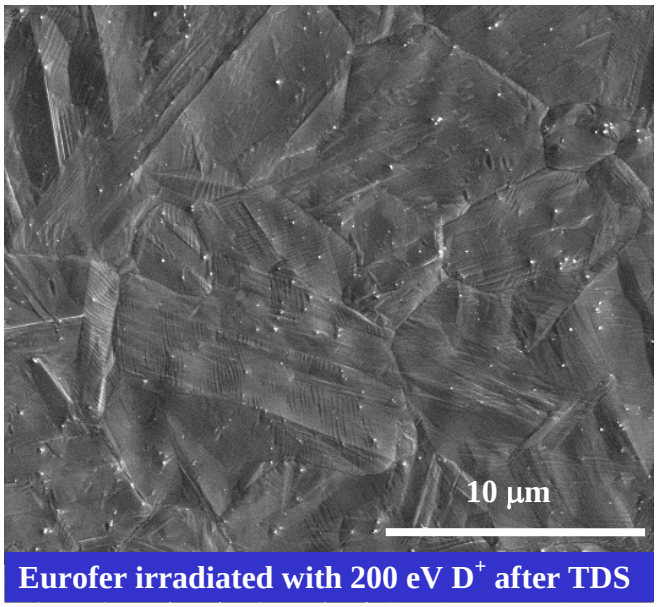

Fig. 7. SEM images of Eurofer after exposure to the D plasma with incident ion energy of 200 eV per D at 290 K (shown in **Fig. 3a**) and then heated in a vacuum up to 1200 K with a linear ramp of 2 K/s.

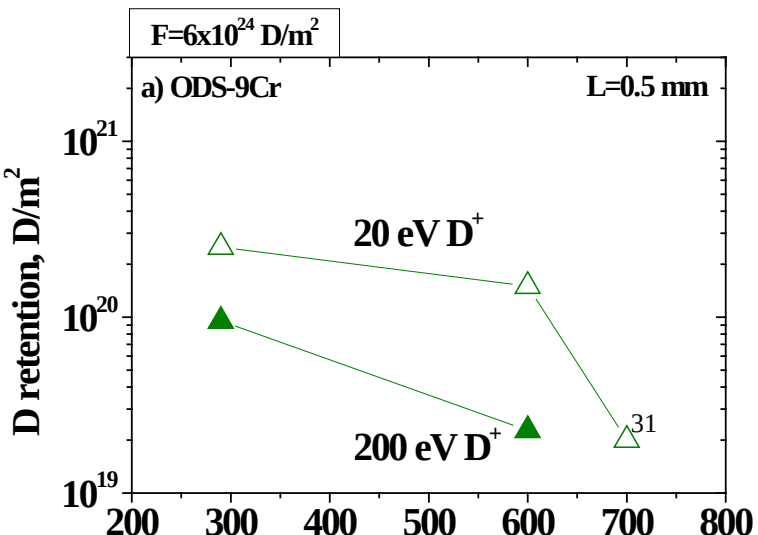

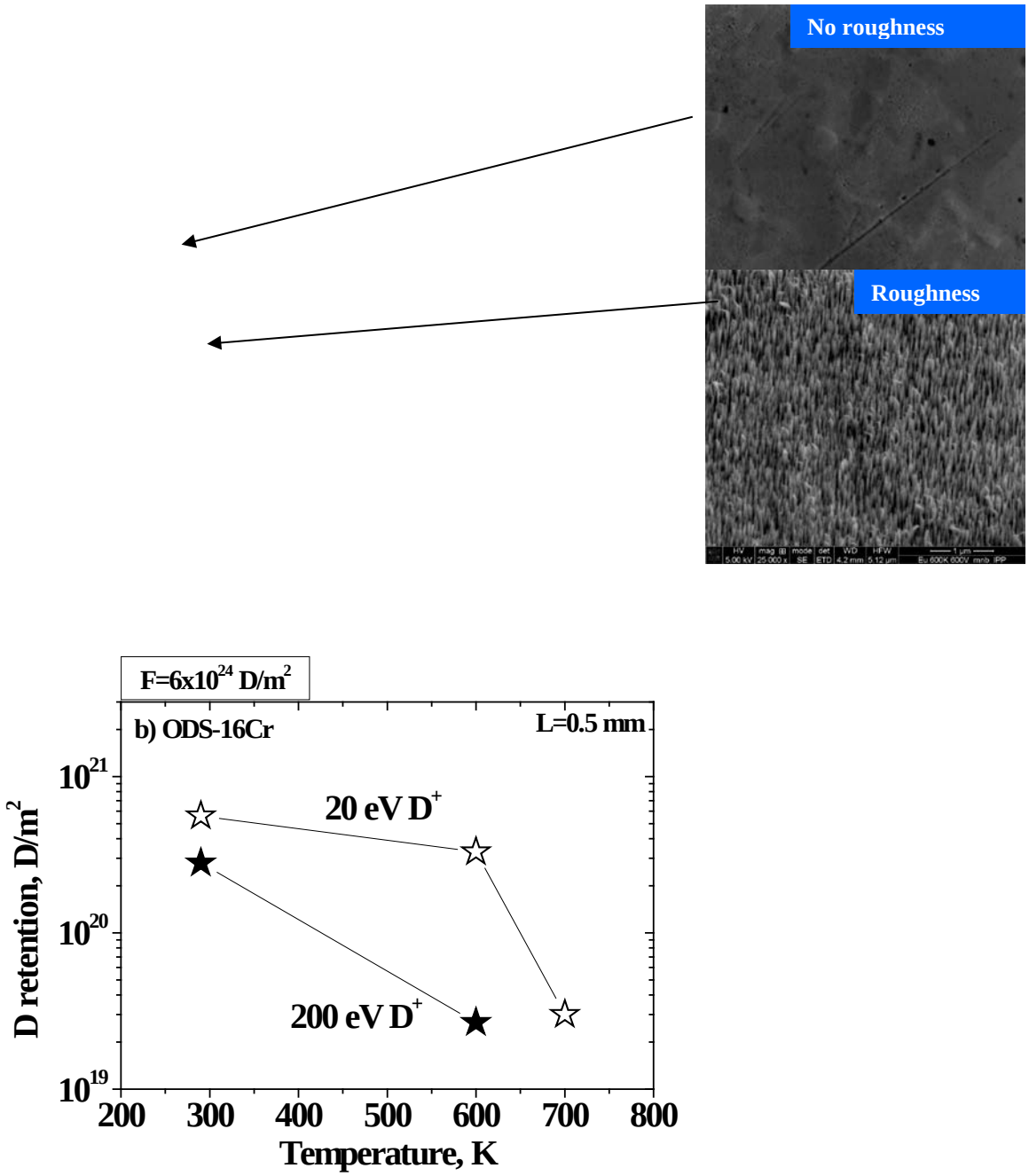

Fig. 8. The D retention obtained by TDS after the D plasma exposure with incident ion energies of 20 and 200 eV per D as a function of the sample temperature under the plasma exposure in the case of a) ODS-9Cr and b) ODS-16Cr. The sample thicknesses were L=0.5 mm and fluence was $6x10^{24}$ D/m^2.

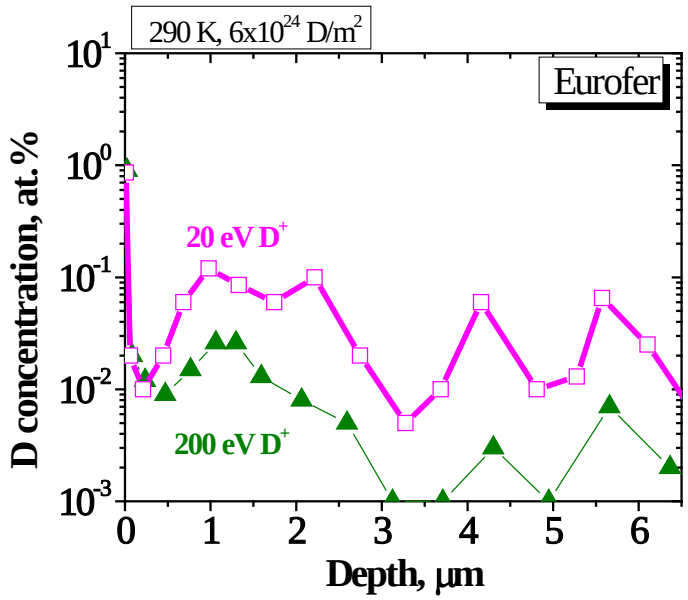

Fig. 9. Depth profiles of the D concentration in Eurofer irradiated with incident ion energies of 20 and 200 eV per D at 290 K up to a fluence of $6x10^{24}$ D/m^2. Sputtered layer is ~1.2 μm.

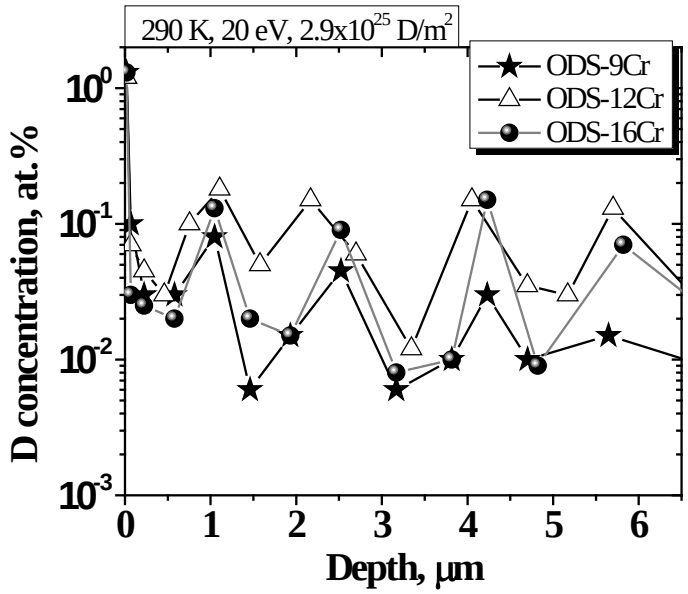

Fig. 10. Depth profiles of the D concentration in ODS with different amount of Cr exposed to the D plasma with incident ion energy of 20 eV per D atom at 290 K up to a fluence of F=2.9x10^{25} D/m^2.

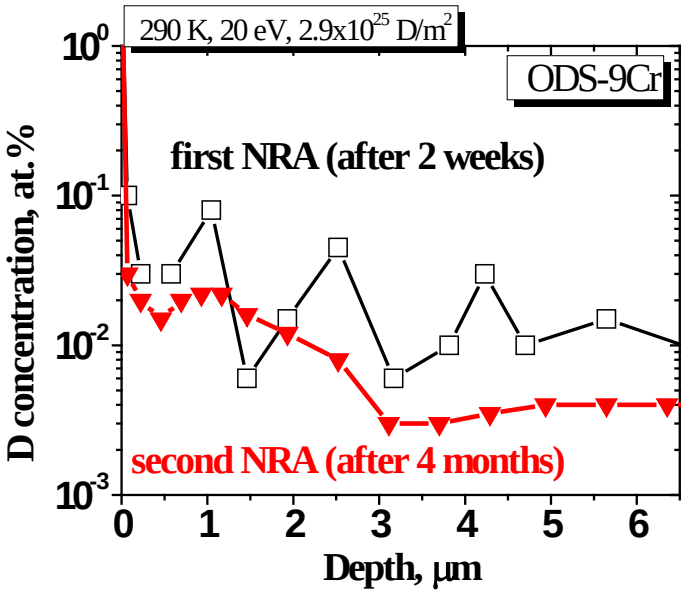

Fig. 11. Depth profiles of the D concentration in ODS-9Cr steel irradiated with incident ion energy of 20 eV per D at room temperature up to a fluence of 2.9×10^{25} D/m^2. The measurements were performed in two weeks and four months after the D plasma exposure.

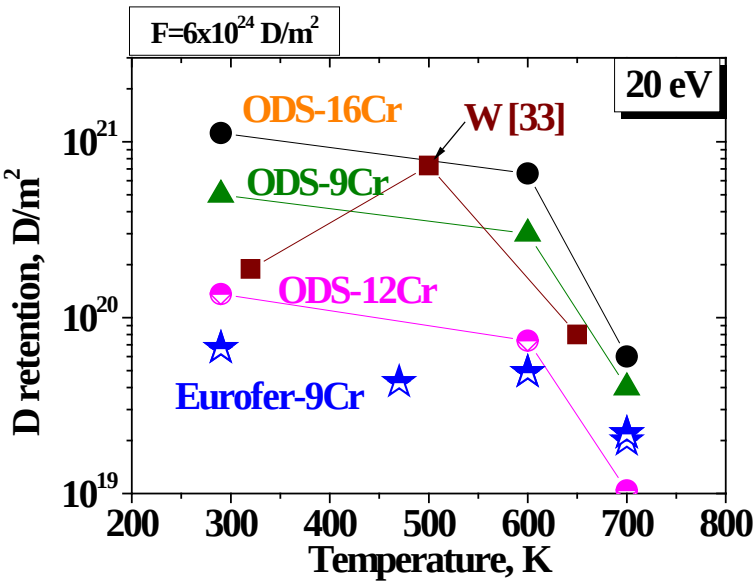

Fig. 12. A comparison of the D retention in Eurofer and ODS steels with different content of Cr with bulk polycrystalline W ITER grade [**33**] measured by TDS after the D plasma exposure with incident ion energy of 20 eV per D up to a fluence of $6x10^{24}$ D/m^2. The sample thicknesses were L=1 mm.

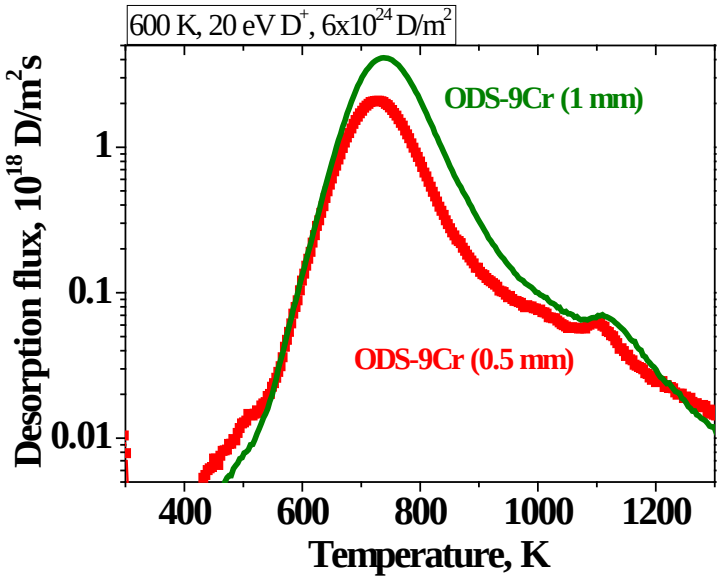

Fig. 13. The thermal desorption spectra of deuterium from ODS-9Cr after the D plasma exposure with incident ion energy of 20 eV per D at 600 K up to a fluence of $6x10^{24}$ D/m^2 at different sample thicknesses of 0.5 and 1 mm.

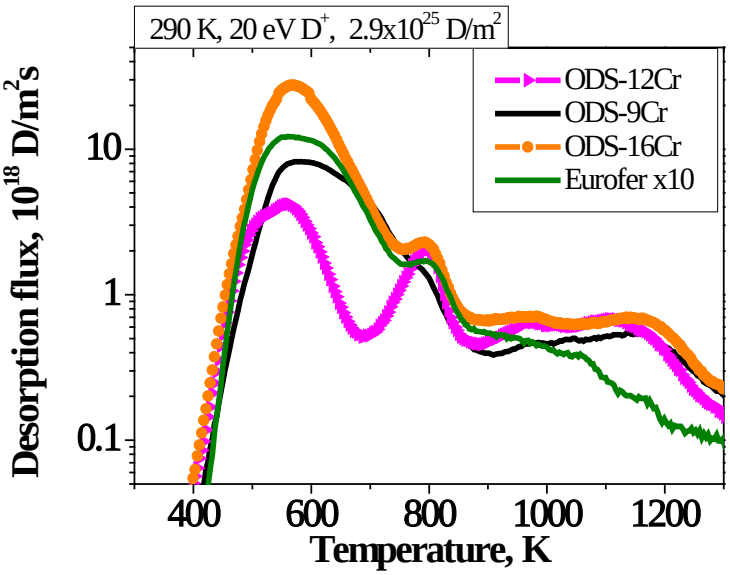

Fig. 14. Thermal desorption spectra of deuterium from steels exposed to D plasma with incident ion energy of 20 eV per D at room temperature up to a fluence of 2.9×10^{25} D/m^2. The TDS for Eurofer is multiplied by a factor of 10.

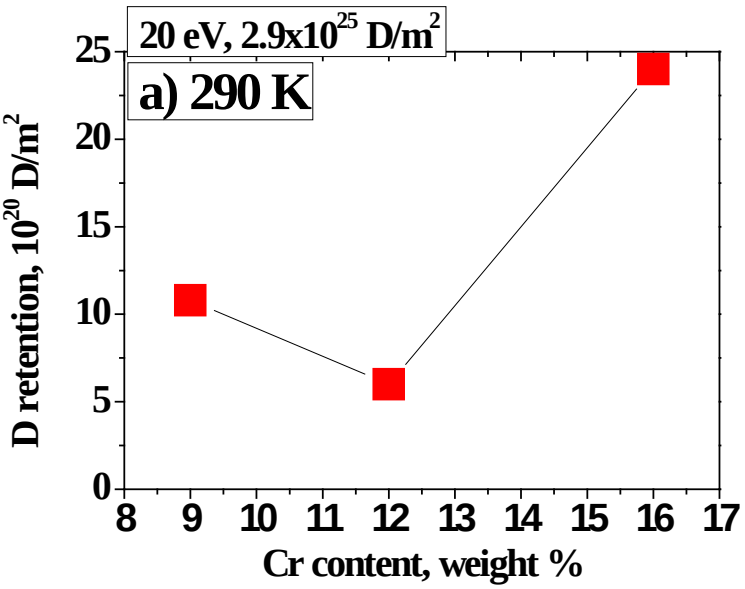
20 eV, 2.9x10^25 D/m^2
a) 290 K
D retention, 10^20 D/m^2
Cr content, weight %

a)

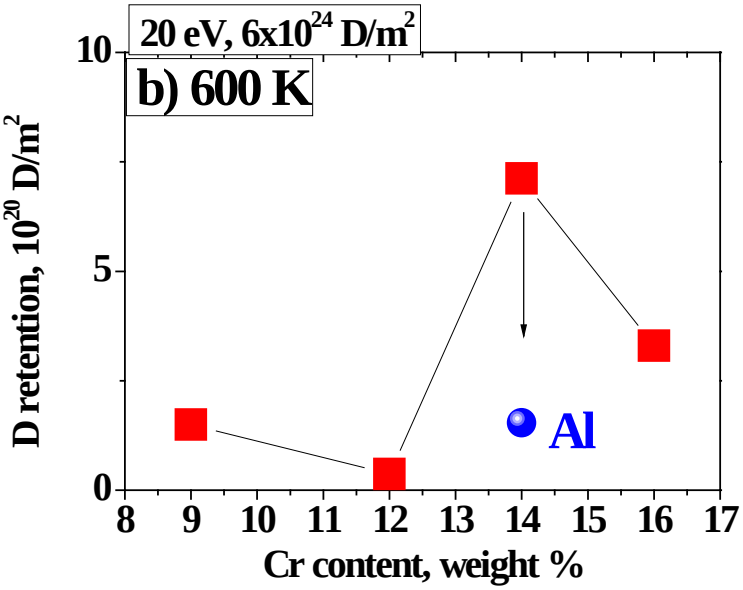
20 eV, 6x10^24 D/m^2
b) 600 K
Al
D retention, 10^20 D/m^2
Cr content, weight %

b)

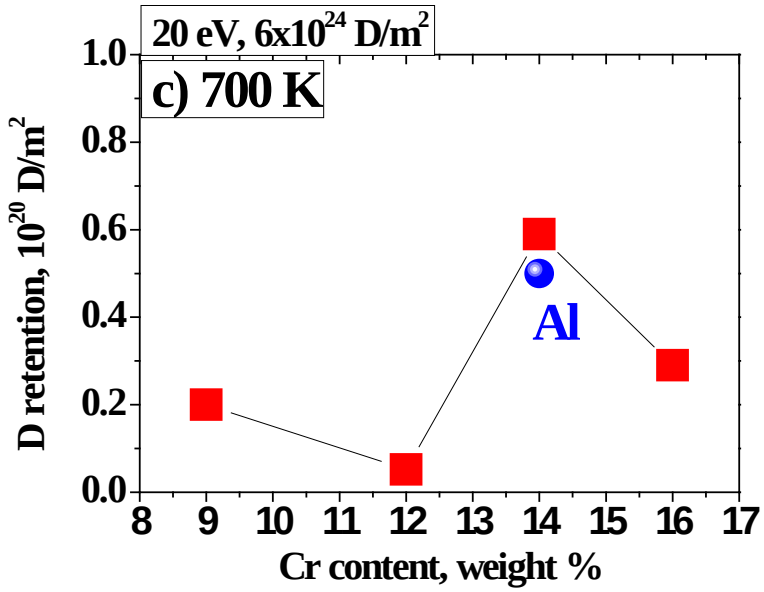

c)

Fig. 15. The dependence of the D retention on the Cr content in ODS steel after exposure to the D plasma with incident ion energy of 20 eV per D at: a) 290 K, b) 600 K and c) 700 K.

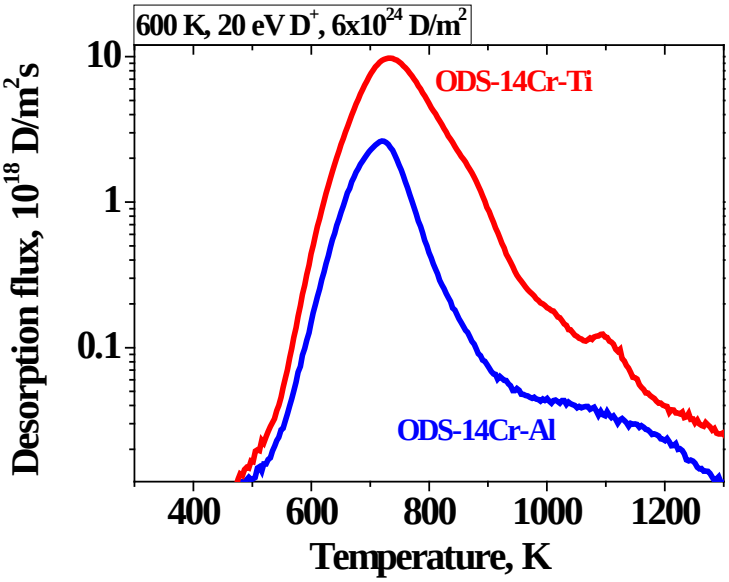

Fig. 16. Thermal desorption spectra of deuterium from ODS-14Cr-Ti and ODS-14Cr-Al steels exposed to D plasma with incident ion energy of 20 eV per D at 600 K.

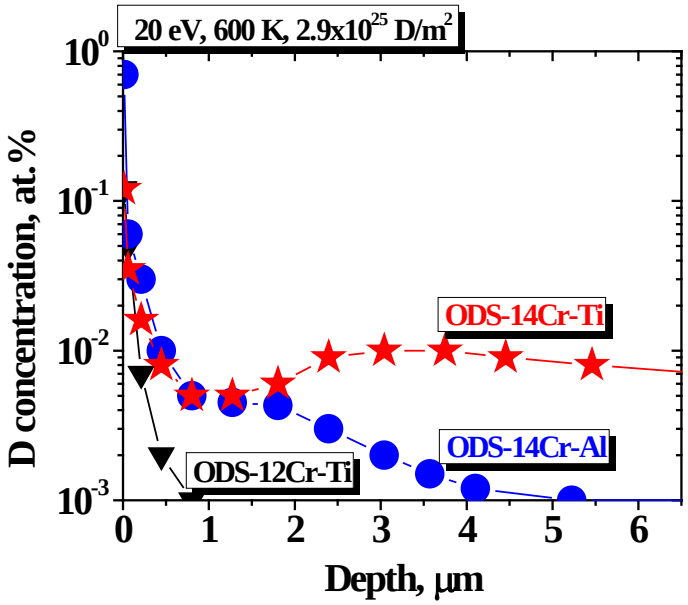

Fig. 17. Depth profiles of the D concentration in ODS steels after exposure to D plasma with incident ion energy of 20 eV per D at 600 K up to a fluence of F=2.9x10^{25} D/m^2.